



Pro-arrhythmic Effects of Hydrogen Sulfide in Healthy and Ischemic Cardiac Tissues: Insight From a Simulation Study

Shugang Zhang^{1,2}, Shanzhuo Zhang³, Xiaoshuai Fan⁴, Wei Wang⁵, Zhen Li^{1,2}, Dongning Jia^{1,2}, Zhiqiang Wei^{1,2*} and Henggui Zhang^{2,4,6*}

¹ Department of Computer Science and Technology, Ocean University of China, Qingdao, China, ² Qingdao National Laboratory for Marine Science and Technology, Qingdao, China, ³ School of Computer Science and Technology, Harbin Institute of Technology, Harbin, China, ⁴ Biological Physics Group, Department of Physics and Astronomy, The University of Manchester, Manchester, United Kingdom, ⁵ School of Computer Science and Technology, Harbin Institute of Technology, Shenzhen, China, ⁶ Key Laboratory of Medical Electrophysiology of Ministry of Education and Medical Electrophysiological Key Laboratory of Sichuan Province, Institute of Cardiovascular Research, Southwest Medical University, Luzhou, China

OPEN ACCESS

Edited by:

Joseph L. Greenstein,
Johns Hopkins University,
United States

Reviewed by:

Zhilin Qu,
University of California, Los Angeles,
United States

Christopher Huang,
University of Cambridge,
United Kingdom

*Correspondence:

Zhiqiang Wei
weizhiqiang@ouc.edu.cn
Henggui Zhang
henggui.zhang@manchester.ac.uk

Specialty section:

This article was submitted to
Computational Physiology
and Medicine,
a section of the journal
Frontiers in Physiology

Received: 15 June 2019

Accepted: 19 November 2019

Published: 13 December 2019

Citation:

Zhang S, Zhang S, Fan X, Wang W, Li Z, Jia D, Wei Z and Zhang H (2019) Pro-arrhythmic Effects of Hydrogen Sulfide in Healthy and Ischemic Cardiac Tissues: Insight From a Simulation Study. *Front. Physiol.* 10:1482. doi: 10.3389/fphys.2019.01482

Hydrogen sulfide (H₂S), an ambient air pollutant, has been reported to increase cardiac events in patients with cardiovascular diseases, but the underlying mechanisms remain not elucidated. This study investigated the pro-arrhythmic effects of H₂S in healthy and ischemic conditions. Experimental data of H₂S effects on ionic channels (including the L-type Ca²⁺ channel and ATP-sensitive K⁺ channel) were incorporated into a virtual heart model to evaluate their integral action on cardiac arrhythmogenesis. It was shown that H₂S depressed cellular excitability, abbreviated action potential duration, and augmented tissue's transmural dispersion of repolarization, resulting in an increase in tissue susceptibility to initiation and maintenance of reentry. The observed effects of H₂S on cardiac excitation are more remarkable in the ischemic condition than in the healthy condition. This study provides mechanistic insights into the pro-arrhythmic effects of air pollution (H₂S), especially in the case with extant ischemic conditions.

Keywords: arrhythmia, air pollution, hydrogen sulfide, ischemia, simulation

INTRODUCTION

Pro-arrhythmia risks of ambient air pollution have been long established by epidemiological evidences. Inflammation, autonomic nervous system (ANS) changes, and pulmonary or systemic oxidative stress are currently recognized as potential factors responsible for arrhythmogenesis of air pollution (Link and Dockery, 2010; Martinelli et al., 2013); however, the specific effect of air pollution on cardiac functions remains incompletely elucidated owing to the complicated composition of air pollutants (Schlesinger, 2007; Mills et al., 2009; Fiordelisi et al., 2017). Hydrogen sulfide (H₂S) is a common air pollutant characterized by an odor of rotten eggs and is largely produced in industrial activities, such as food processing, coke ovens, and petroleum refineries. Although epidemiological research has shown association between ambient H₂S and cardiovascular disease hospitalization and mortality (Godleski et al., 2000; Bates et al., 2002; Finnbjornsdottir et al., 2015, 2016), how it affects the functions of the cardiovascular system is unclear.

Recent studies at the cellular level suggested that NaHS (H_2S donor) can significantly shorten the action potential duration (APD) of cardiomyocytes, possibly by affecting the ATP-sensitive K^+ channel (K-ATP) (Bian et al., 2006; Johansen et al., 2006; Zhang et al., 2007; Abramochkin et al., 2009; Chan et al., 2018) and the L-type Ca^{2+} channel (Ca-L) (Sun et al., 2008; Zhang et al., 2012). Experiments on rats have characterized the dose-dependent effects of NaHS on ionic currents of the two channels, I_{CaL} and $I_{\text{K,ATP}}$ (Sun et al., 2008; Zhong et al., 2010), and suggested that low doses of NaHS (i.e., 100 and 150 $\mu\text{mol/L}$) abbreviated APD by either an enhanced $I_{\text{K,ATP}}$ (Zhong et al., 2010) or a reduced I_{CaL} (Sun et al., 2008). Although it is possible that other channel currents may be involved in their experiments owing to the use of a high concentration of intracellular ATP or channel blockers, it is unclear if the observed increase in $I_{\text{K,ATP}}$ or decrease in I_{CaL} is sufficient to account for the abbreviation of the APD by NaHS.

It is unclear either how NaHS affects the conduction of action potential (AP) through the transmural ventricular wall. It is known that regional difference of cellular property exists in transmural ventricle cells, and such regional difference in cellular property may be altered by NaHS by modulating the intrinsic transmural dispersion of APD and the effective refractory period (ERP) of cardiac tissues, leading to increased tissue susceptibility to arrhythmogenesis. In addition, in ischemic condition, cardiac electrophysiology is remodeled (Shaw and Rudy, 1997; Tr n r et al., 2007; De Diego et al., 2008). It is unclear how NaHS affects the conduction of electrical excitation waves in ischemic tissues and modulates the transmural ERP dispersion, leading to an increased pro-arrhythmic effect.

This study aimed to use a mathematical model of the heart (virtual heart) to evaluate the functional impact of H_2S /NaHS-induced changes in I_{CaL} and $I_{\text{K,ATP}}$ on the electrical properties of rat ventricular myocardium. Specifically, we modified the Pandit et al. (2001) model of healthy rat ventricular myocytes by incorporating $I_{\text{K,ATP}}$ and actions of NaHS on I_{CaL} and $I_{\text{K,ATP}}$. Using the model, we simulated the effect of NaHS on cardiac excitation in both control and ischemic conditions with considerations of ischemia-induced alterations to cellular and tissue properties based on available experimental data. Using cellular models, effects of NaHS on cellular AP, excitability, APD, ERP, and transmural dispersion of ERP (ΔERP) were computed. Using one-dimensional (1D) model of a transmural ventricular tissue strand, effects of NaHS on ventricular conduction and susceptibility to arrhythmogenesis were also investigated. Finally, effects of NaHS on the genesis and maintenance of reentrant arrhythmias in a two-dimensional (2D) transmural ventricular sheet model were quantified.

RESULTS

Effects of NaHS on Action Potentials via Changes in Individual Ion Channels

The effects of NaHS by its action on I_{CaL} alone are shown in **Figure 1**. In simulations, the inhibition action of 100 $\mu\text{mol/L}$ NaHS on I_{CaL} was simulated by Eq. 3, whereas the $I_{\text{K,ATP}}$

was simulated based on Eq. 2 with the a ratio of intracellular ATP:ADP being kept normoxic as in Sun et al. (2008) (see section “Materials and Methods”). It was shown that a decreased I_{CaL} by NaHS abbreviated the APD for both endocardial (**Figure 1A**) and epicardial (**Figure 1B**) cells, with no marked effect on their amplitude or the resting potential. Such simulated changes qualitatively matched with experimental data of Sun et al. (2008), although there are some quantitative discrepancies between simulation and experimental data (**Figure 1C**), possibly owing to a greater I_{CaL} current density in the Pandit model (around -11 pA/pF) as compared with the experimental data (only -3.21 ± 0.13 pA/pF), which produced a greater APD abbreviation than the experimental data of Sun et al. (2008).

The effects of NaHS on $I_{\text{K,ATP}}$ alone are illustrated in **Figure 2**. In this case, the action of NaHS on $I_{\text{K,ATP}}$ was calculated from Eq. 2 (see section “Materials and Methods”) with a ratio of intracellular ATP:ADP as 200:4.5 for anoxic myocytes to mimic the low ATP experimental setting. It was shown that the simulated hypoxic condition abbreviated APD in both the endocardial (**Figure 2A**) and epicardial (**Figure 2B**) cells with the ATP:ADP setting as stated above. The simulated APD abbreviation of both cell types was consistent with experimental data of Zhong et al. (2010) (**Figure 2Cii**), although no specific cell type was identified in their experimental study.

Effects of NaHS on APs

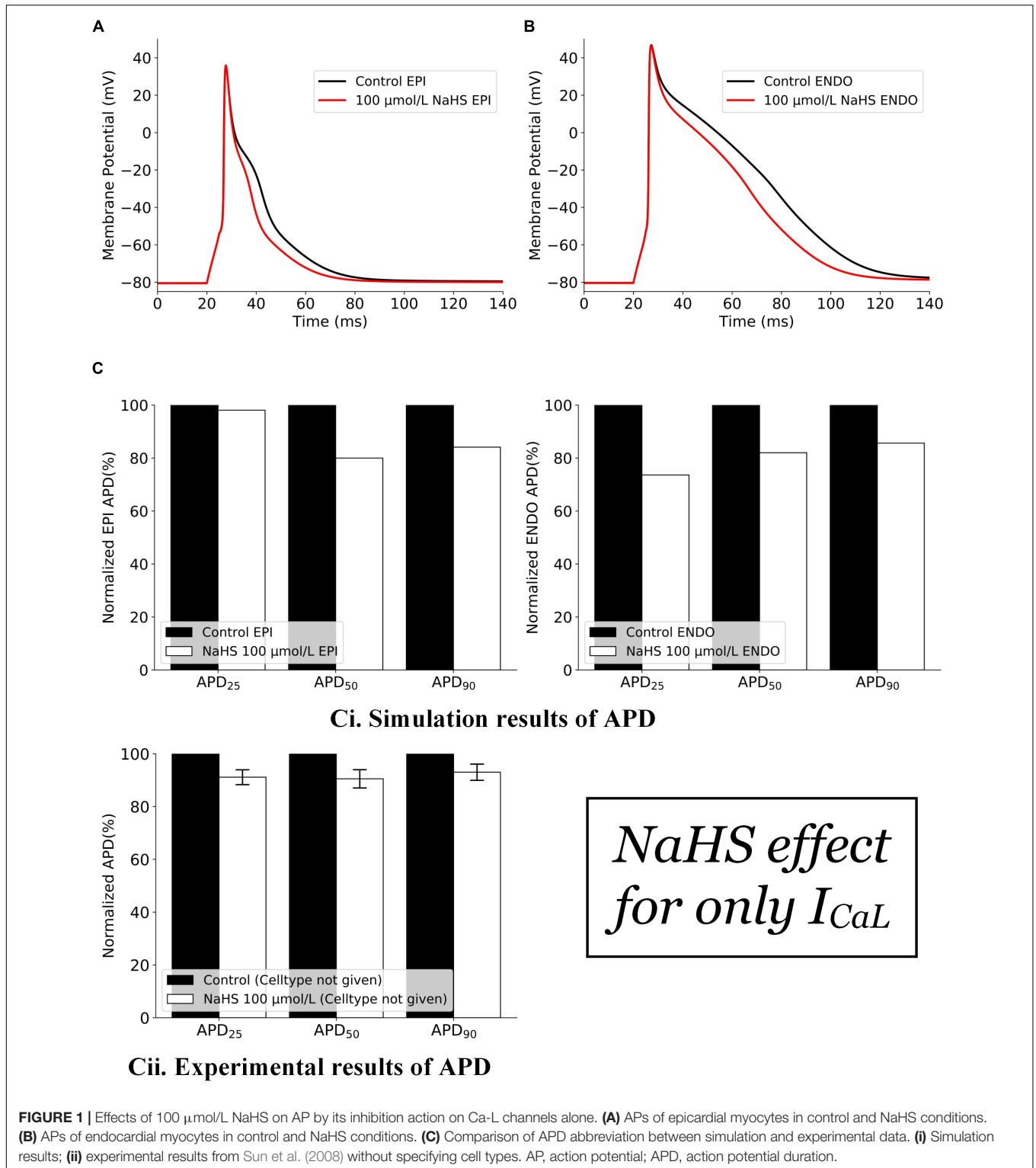
The effects of NaHS on the electrical APs of cardiac cells by integral actions of a reduced I_{CaL} and an enhanced $I_{\text{K,ATP}}$ are presented in **Figure 3**. NaHS shortened the APD for both endocardial and epicardial cells (**Figures 3A,B**). Note that the results presented in **Figures 3A,B** are similar to those shown in **Figure 1**, where the $I_{\text{K,ATP}}$ was blocked by a high concentration of the intracellular ATP, suggesting that the observed APD shortening by NaHS was mainly attributable to the reduced I_{CaL} .

Effects of NaHS in Ischemic Myocytes

NaHS may modulate differently the electrical activity of cardiac cells between ischemic and healthy conditions. To test this hypothesis, further simulations were conducted to evaluate the effect of NaHS on APs of ischemic cells, and results are shown in **Figures 3C,D**. Similar to the healthy condition, NaHS abbreviated APD for both endocardial and epicardial cells; however, it showed a greater APD abbreviation in endocardial than in epicardial cells. Such an observation reflects different electrophysiological responses of endocardial and epicardial cells to the same dose of NaHS. The use of 100 $\mu\text{mol/L}$ NaHS barely affected the resting potential but decreased the AP amplitude (APA) of ischemic cells, which was more marked in the endocardial cell model.

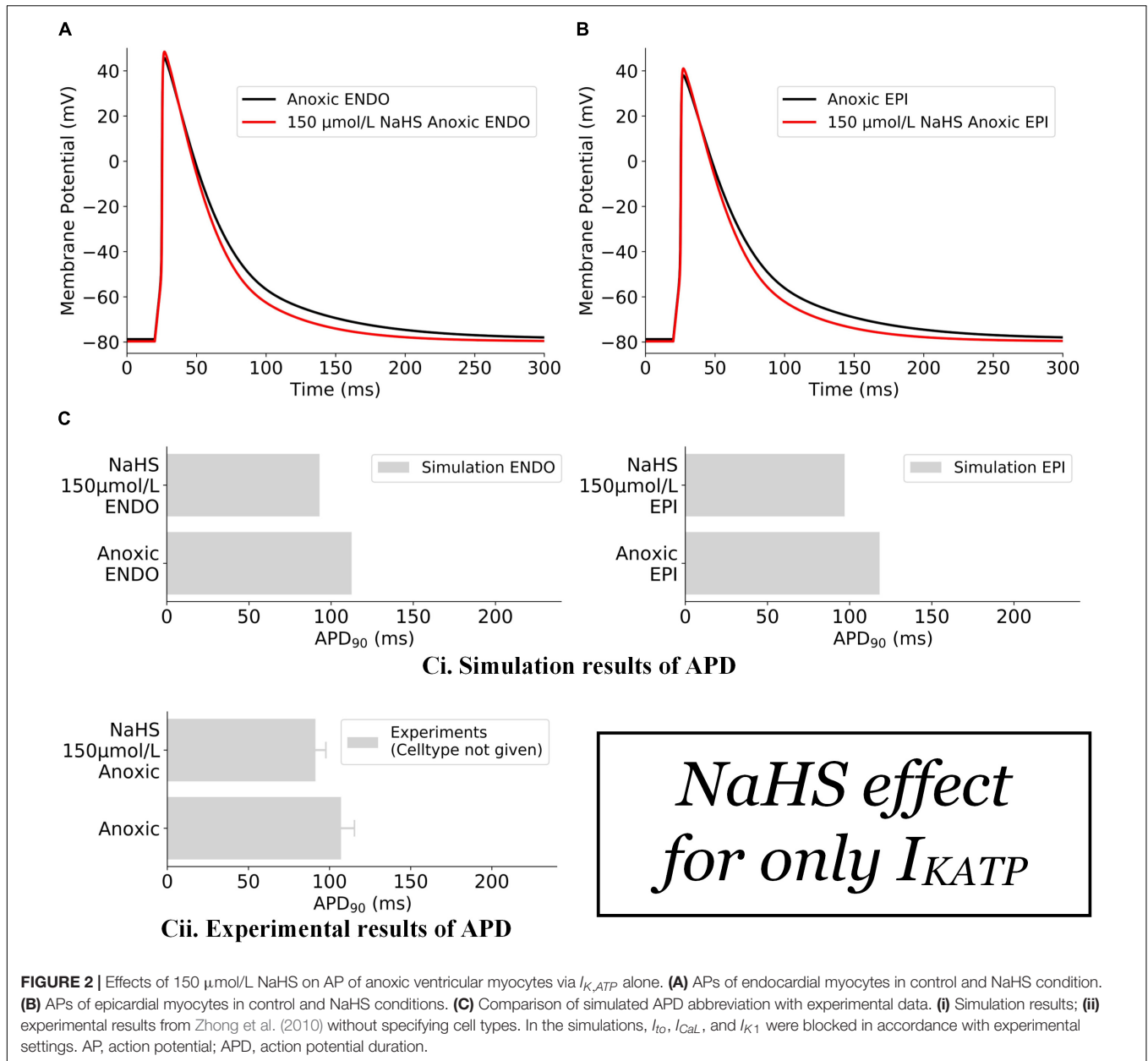
Effects of NaHS on Cellular Refractoriness and Excitability

The effects of NaHS on cellular APD and ERP, and the differences between the endocardial and epicardial cells are shown respectively in **Figures 3E–G**. NaHS abbreviated APD for both endocardial and epicardial cells in healthy and ischemic



conditions; however, it had a different effect on ERP between ischemic and healthy conditions – NaHS decreased the ERP in healthy myocytes but increased it in ischemic myocytes. Such different effects of NaHS on modulating APD and ERP were attributed to the involvement of NaHS- $I_{K,ATP}$, which suppressed

the upstroke and amplitude of the AP, leading to a prolonged ERP in the ischemic condition. A non-uniformly modulated ERP between endocardial and epicardial cells produced an augmented ERP dispersion across the transmural ventricular wall, as illustrated in **Figure 3G**, with the measured transmural



gradient of ERP increased by 3.1% and more significantly in the ischemic ventricular wall with ΔERP increased by 32.5%.

Further analyses were conducted to study the effect of NaHS on cellular excitability, measured reciprocally by the threshold of an external stimulus to evoke an AP. Results are shown in **Figures 3I,J** for the control and ischemic conditions with a low dose of NaHS at 100 $\mu\text{mol/L}$. In the healthy condition, NaHS did not affect the measured excitation threshold for either the endocardial or epicardial cell model but increased it in the ischemic condition, suggesting that NaHS reduced cellular excitability in the ischemic condition.

Note that the measured excitation threshold of the endocardial and epicardial cell models was affected by the ischemic condition, which is dependent on the S1–S2 intervals. In the ischemic

condition, compared with the healthy condition, the measured threshold was lower at long intervals whereas greater at short intervals. Such a difference in the modulated cellular excitability by the ischemic condition was attributable to the combined effect of a prolonged ERP and a more depolarized resting potential as seen in the ischemic condition. Whereas the former increased the excitation threshold at short intervals, causing a rightward shift of the measured threshold curve (**Figures 3I,J**), the latter reduced the excitation threshold owing to a closer distance between the depolarized resting potential by ischemia and the threshold potential, which is easier to evoke an AP. However, if the resting potential was further elevated by more severe hyperkalemia and finally exceeded the threshold potential, it would always be harder to evoke an AP (i.e., a bigger excitation

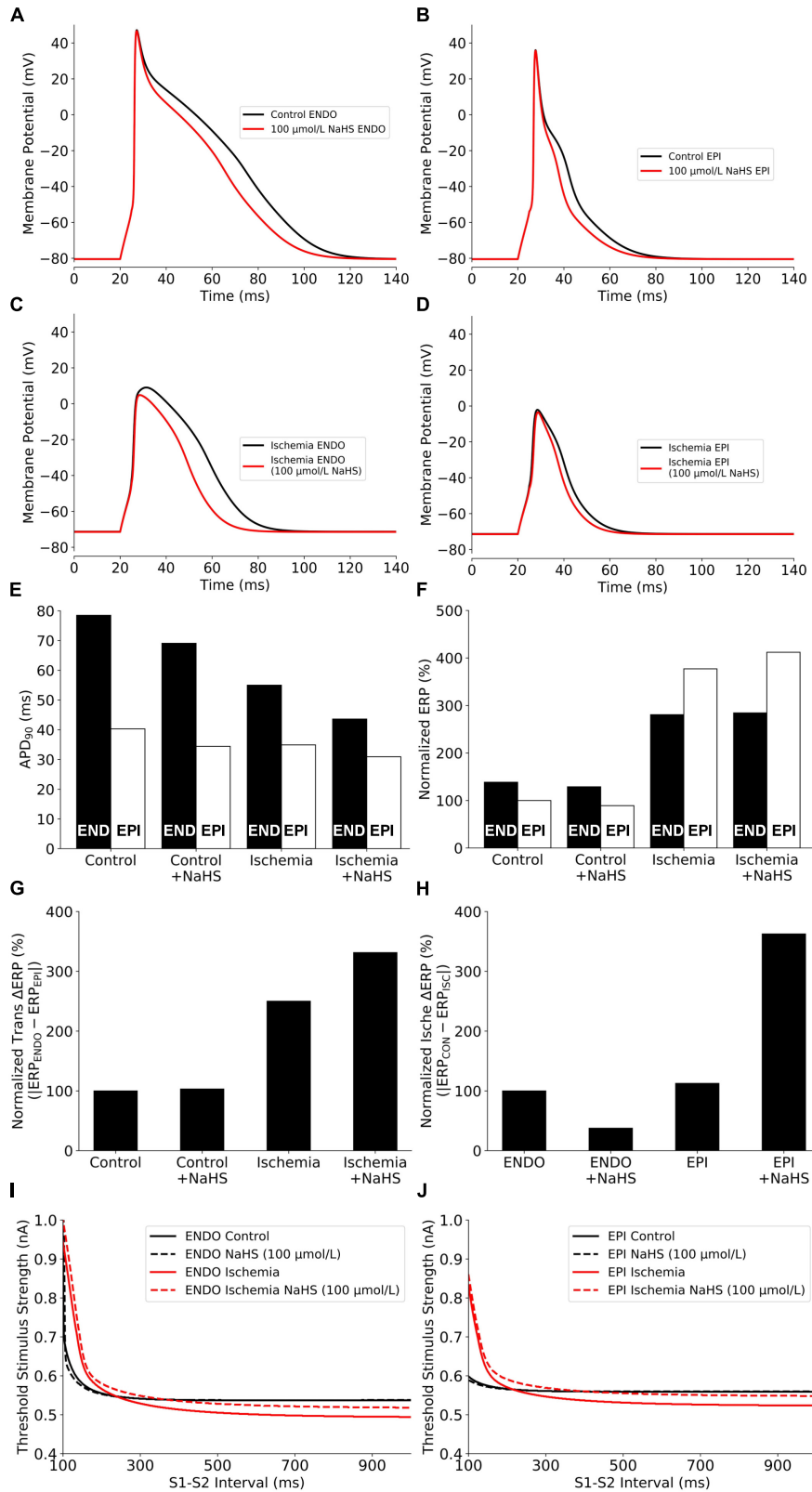
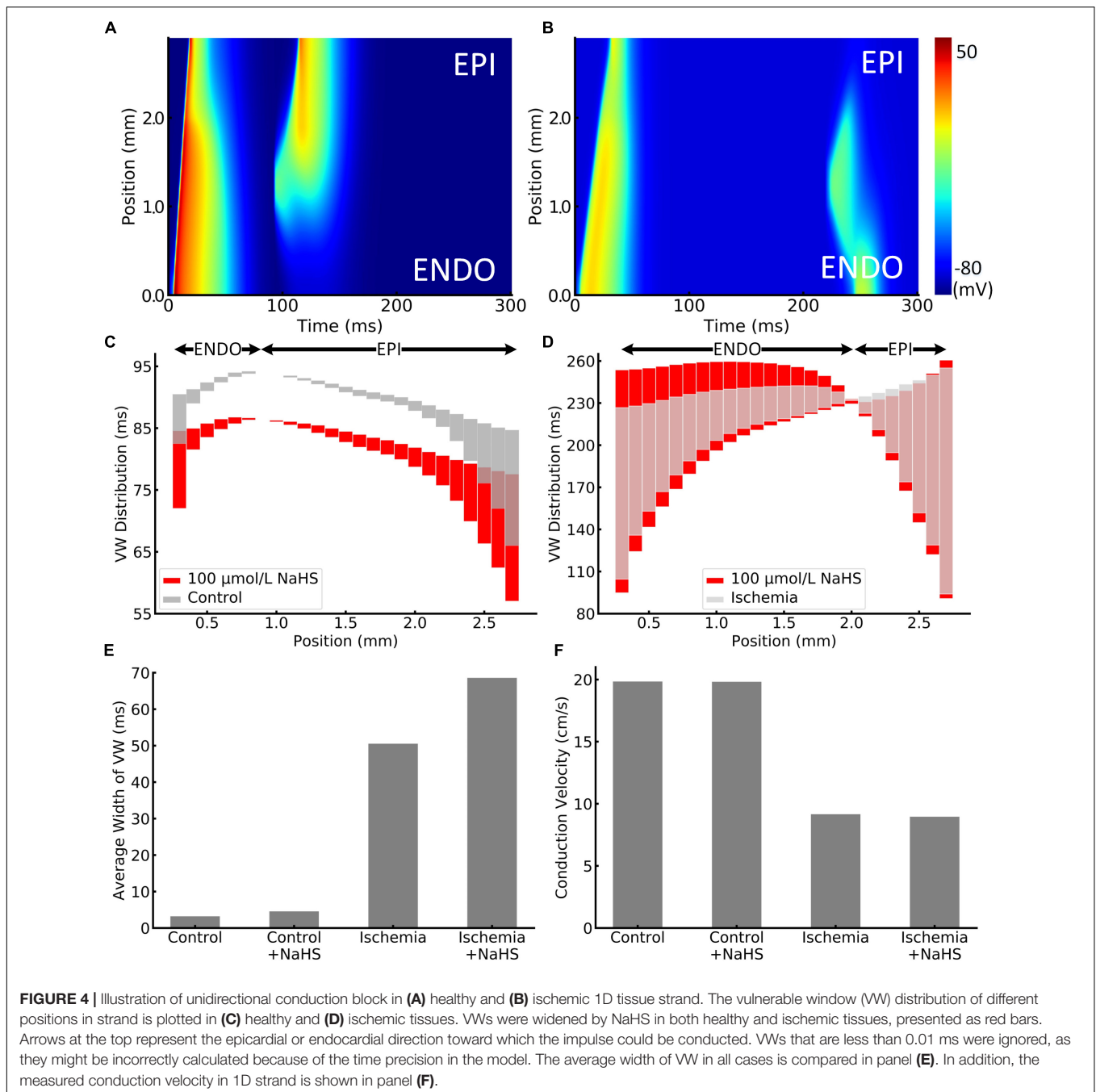


FIGURE 3 | Summary of the effects of NaHS and ischemia on (A–D) AP morphology, (E) APD₉₀, (F) Normalized ERP, (G) Normalized ERP transmural gradients between epicardial/endocardial cells, (H) Normalized ERP gradients between ischemic/non-ischemic cells, and (I,J) excitability. AP, action potential; APD, action potential duration; ERP, effective refractory period.



threshold) in ischemia than in healthy myocyte regardless of the S1–S2 interval.

Temporal Vulnerability to Unidirectional Conduction Block

The effect of NaHS on tissue's vulnerability to genesis of unidirectional conduction block in response to a premature stimulus was also evaluated. **Figures 4A,B** presented examples of the simulated unidirectional conduction block in healthy and ischemic tissues. **Figure 4A** clearly shows that owing to the

shorter APD in the epicardial region as compared with the endocardial portion, the S2 stimulus applied to the epicardial region (1.0–1.6 mm from the endocardial portion) produced an anterograde conduction. However, the same premature stimulus applied to the same location produced unidirectional conduction in the retrograde direction in ischemic tissues, owing to a reduced conduction velocity (CV) and the altered effective refractory properties. Unidirectional conduction block can only be induced at a certain time period (termed *vulnerable window* [VW]), or bidirectional block/propagation will happen. The computed overall distribution of VW across the tissue strand is shown in

Figures 4C,D, where the light gray bars and red bars are the VW distribution with and without NaHS. The black arrows in these two panels indicated the direction of the unidirectional conduction evoked by the premature S2 stimulus, showing a change in the conduction direction. In healthy tissues, the direction of conduction changed at around 0.7 mm from the endocardial portion, and it happened in a more forward position around 1.9 mm in the ischemia case (**Figure 4D**). The average width of VW in four conditions is plotted in **Figure 4E**, in which it can be seen that ischemia greatly increased the width of the VW by nearly 16 times from 3.2 to 50.5 ms. Marked width of VW across the whole strand suggested a highly increased tissue susceptibility to unidirectional block in the ischemic condition.

When applying 100 $\mu\text{mol/L}$ of NaHS, the width of VW was increased in both healthy and ischemic conditions, and the phenomenon was more significant in the ischemic tissues. Specifically, NaHS further increased the average width of VW from 50.5 to 68.6 ms in the ischemia condition, whereas it slightly increased the average VW width from 3.2 to 4.6 ms in healthy tissues (see **Figure 4**). The above observation suggested that NaHS could contribute to even higher risks in the ischemic tissues that are already fragile and susceptible to unidirectional block. The adverse effect of NaHS was observed in all locations throughout the strand notwithstanding the direction of conduction. **Figure 4F** presents the comparison of CV, where NaHS barely affected the CV in healthy tissues with only 0.1% decrement from 19.84 to 19.82 cm/s. In ischemic tissues, NaHS decreased the CV by 2.1% from 9.16 to 8.96 cm/s.

Spatial Vulnerability of Tissue to Sustain Reentry

The effects of NaHS on the dynamic behavior of reentrant excitation waves were also investigated. Premature stimulus during the VW in 2D tissues led to a unidirectional propagation of the impulse toward the anterograde direction, and this impulse further evolved into a spiral wave, as shown in **Figure 5**. After initiation of the spiral wave, it required a minimum tissue's substrate to sustain, the *critical length* of which can be used as an index to quantify tissue susceptibility for maintaining reentry. In the healthy condition, the measured critical length was 7.7 mm (**Figures 5Ai–Aviii**), which decreased by almost 30% to 5.4 mm in the early phase of ischemic tissues (**Figures 5Bi–Bviii**). This was attributed to the reduced CV and APD in ischemic tissues, producing a short wavelength and thus facilitating the survival of the paired spiral waves.

NaHS measuring 100 $\mu\text{mol/L}$ decreased the critical length in both healthy tissues and ischemic tissues (**Figure 5C**), which was also attributable to the shortening of APD and wavelength of excitation.

Dynamics of Spiral Waves

Spiral waves in the 2D model of transmural ventricular tissues were unstable in both healthy and ischemic tissues, leading them to self-termination with a finite life span. As shown in **Figure 5D**, in the healthy tissues, the life span of spiral wave was about 220 ms, which was prolonged to 232 ms by NaHS.

In the tissue model with early phase of ischemia, the life span of spiral wave was about 151 ms, which changed to about 139 ms in the NaHS condition.

DISCUSSION

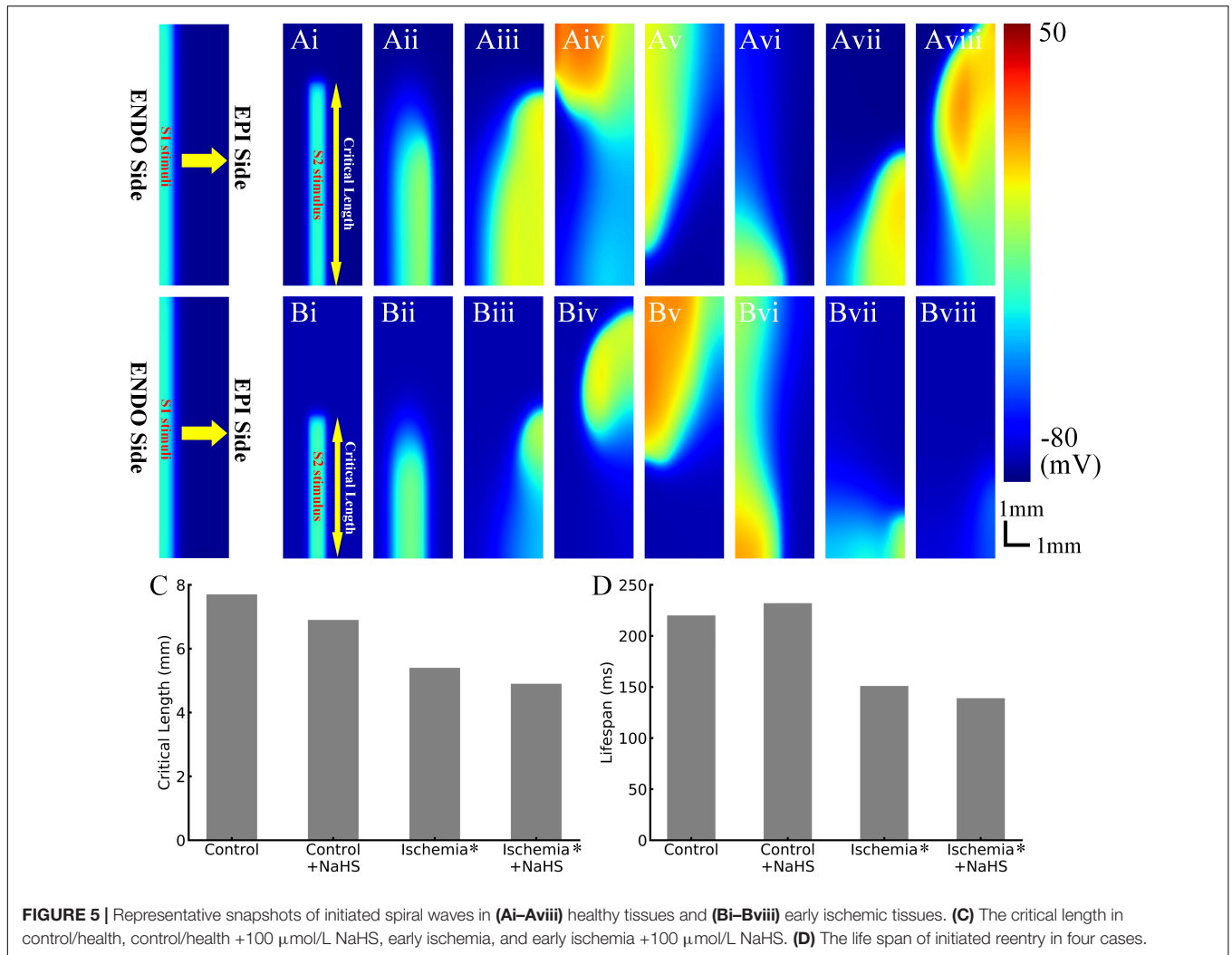
Although the common industrial air pollutant H_2S is hazardous to human cardiovascular system, its underlying mechanisms have not been elucidated yet. In this study, we computationally investigated the functional influence of H_2S on cardiac electrical excitations in healthy and ischemic conditions on the basis of experimental data of NaHS (a donor of H_2S). Our major findings are as follows: (i) at the cellular level, NaHS shortens APD, which was more significant in the ischemia condition, whereas it decreased ERP in healthy but increased it in the ischemic condition; (ii) NaHS augmented the ERP difference between epicardial and endocardial myocytes (i.e., ΔERP) in both healthy and ischemia conditions and augmented the ERP difference between ischemic and non-ischemic cells; (iii) at the tissue level, it increased tissue vulnerability for initiation and maintenance of reentry, which is more significant in the ischemic condition. It also prolonged the life span of reentry. All taken together, these findings provide explanations to the pro-arrhythmic effects of H_2S , especially in the ischemic conditions.

Mechanisms of Pro-arrhythmogenesis Action Potential Duration and Effective Refractory Period Abbreviation

NaHS shortens APD in both healthy and ischemic myocytes through an integrated action of depressed I_{CaL} and enhanced $I_{\text{K,ATP}}$. In simulation, APD abbreviation was more obvious in ischemia owing to more opened K-ATP channels. However, changes of ERP were different in these two situations, whereas NaHS decreased the ERP in healthy myocytes but increased it in ischemic myocytes, which is also attributable to the involvement of $I_{\text{K,ATP}}$ in ischemia (but not in health) that enhanced the repolarization current and reduced the amplitude of APs. NaHS thus prolonged the ERP of ischemic myocytes through its action on increasing $I_{\text{K,ATP}}$.

NaHS Augmented the Effective Refractory Period Dispersion

The transmural dispersion of ERP, measured by the ERP difference (i.e., ΔERP) between epicardial and endocardial myocytes, was augmented by NaHS in both healthy and ischemia conditions. In the healthy condition, NaHS augmented ΔERP as it decreased ERP more in the epicardial cells (by 9 ms) than in endocardial cells (by 8 ms) (see **Figure 3F**), resulting in a 1-ms increment in transmural ΔERP (**Figure 3G**). In the ischemia condition, NaHS also increased ΔERP but not in the same way as in healthy tissues. Instead, NaHS increased the ERP in both cell types as the $I_{\text{K,ATP}}$ was involved in the ischemia condition. However, such ERP increasing effect was more significant in epicardial myocytes (up to 29 ms) than in endocardial myocytes (only 3 ms), as illustrated in the two data groups in the right side of **Figure 3F**. The unevenly altered ERP in epicardial



and endocardial cells contributed to a great enhancement of transmural ΔERP and further increased it by 26 ms. In addition, NaHS also increased the ERP difference between ischemic and non-ischemic epicardial myocytes (Figure 3H). The observation suggested another potential pro-arrhythmic influence of NaHS when local ischemia happened, as the ERP dispersion between the local ischemic areas and the other healthy areas in the epicardium would possibly lead to arrhythmogenesis.

Increased Tissue Vulnerability for Arrhythmogenesis

The augmented repolarization dispersion by NaHS led to the increased temporal vulnerability of tissue to unidirectional conduction block in response to a premature stimulus (Figure 4). In addition, NaHS decreased the CV of excitation waves, which also contributed to the increased width of the measured VW that was exacerbated by the ischemic condition.

Decreased Minimal Substrate Size to Sustain Reentry

NaHS decreased the critical length in healthy and ischemic tissues for sustaining reentry, suggesting an important role in facilitating reentrant arrhythmia. This can be attributable to the abbreviated

APD and ERP, resulting in a shorter excitation wavelength that reciprocally characterizes the spatial vulnerability of tissues (Rensma et al., 1988; Zhang et al., 2008).

Increased Life Span of Reentry

NaHS prolonged the life span of reentry in healthy tissues but not in ischemia. Owing to a limited tissue size (only 3 mm in transmural width) in this study, the initiated spiral wave always self-terminated with finite life span, which was determined by the interplay between the refractory distance of reentry and the transmural ERP gradient of the tissues. In one way, a short refractory distance (can be simply defined as the product of CV and ERP) of an excitation wave needs a small tissue size for accommodating the leading circle of reentry (Comtois et al., 2005), which helps to sustain the reentry. In the other way, the transmural gradient of ERP induces the tip of reentry to drift – a larger ERP gradient produces a more meandering of the tip to run out of the boundary, leading to self-termination. In our simulation, the spiral wave self-terminated in the control case owing to the intrinsic ventricular heterogeneity. NaHS decreased the refractory distance but did not increase the ERP gradient too

much, and the two factors together resulted in a prolonged life span of reentry.

In the ischemic condition, the depressed excitability led to a prolonged ERP, and the refractory distance was enlarged despite a decreased CV. In addition, the augmented ERP dispersion also contributed to the termination of the spiral wave by accelerating the drifts. In this case, these factors interplayed, resulting in a shorter life span of spiral wave in ischemic tissues. NaHS further prolonged ERP by enhancing $I_{K,ATP}$, and it also increased the ERP dispersion; these effects together terminated the spiral wave earlier.

Potential Limitations of This Study

The limitations of the Pandit et al. (2001) model were discussed elsewhere (Terkildsen et al., 2008; Gattioni et al., 2016). In the simulations, the effects of H₂S on cardiac ion channels were based on experimental data of a H₂S donor, NaHS, as NaHS is superior to the direct administration of H₂S for dose control, data reproducibility, and negligible effects on the cellular Na⁺ concentration and pH (Zhong et al., 2003, 2010).

In single-cell model development, data on the effects of NaHS on I_{CaL} and $I_{K,ATP}$ were based on extant data from rats as much as possible to avoid potential species dependence (Furukawa et al., 1991). However, it should be of concern that the interspecies differences regarding the transmural $I_{K,ATP}$ may exist. For example, experiments conducted on rabbit (Qi et al., 2000) or cat (Furukawa et al., 1991) showed a greater $I_{K,ATP}$ activation in epicardial cells than in endocardial cells, but this is not applicable to rats according to the rat experiments (Shimokawa et al., 2007), which reported smaller half-maximal channel inhibition (IC₅₀) of $I_{K,ATP}$ -ATP curve using either inside-out patch recordings or open cell-attached patch recordings, suggesting less $I_{K,ATP}$ activation in epicardial cells than endocardial cells when facing the same decrement of intracellular ATP. Owing to the uncertainty of interspecies difference as well as the insufficient experimental data regarding transmural $I_{K,ATP}$ difference in rats, the transmural heterogeneity of $I_{K,ATP}$ was not incorporated in this study, and the conclusion should be carefully interpreted in clinical study considering the significant electrophysiological differences between human and rats. In 2D simulations, we only considered an earlier phase of ischemia as it was difficult to initiate the spiral wave in a tissue with conditions of 10-min ischemia. Specifically, the largely increased ERP led to a rather large leading circle that required large tissue size for spiral wave tip's meandering, and the limited size of a rat's transmural tissues will no longer be able to accommodate the spiral wave in the late phase of ischemia; thus, we did not conduct the simulation on tissues with conditions of 10-min ischemia.

Note that ischemia will also create the ERP dispersion between ischemic and non-ischemic areas, and NaHS could further enhance the dispersion in the epicardium. The role of such augmented ERP dispersion around the "border zone" of ischemic region may be pro-arrhythmic (Picard et al., 1999; Bernus et al., 2005; Trénor et al., 2007). In the presence of NaHS, how it increases the vulnerability of tissue to cardiac arrhythmias warrants future study.

CONCLUSION

The pro-arrhythmic effects of H₂S arise as a consequence of different alterations of electrical properties in epicardial and endocardial myocytes through modest changes in ion channel conductance, resulting in abbreviated ERP, augmented transmural ERP dispersion, and depressed cell excitability, leading to increased tissue susceptibility for initiation and maintenance of cardiac arrhythmia. The pro-arrhythmic effect of H₂S was more significant in ischemic tissues, providing a novel insight into higher risks among cardiac ischemia population to H₂S-induced ventricular arrhythmias.

MATERIALS AND METHODS

Modeling K-ATP Channel in Epicardial and Endocardial Myocytes

We used a detailed mathematical model of K-ATP channel developed by Ferrero et al. (1996). More details of the model can be found in the **Supplementary Material**. Briefly, $I_{K,ATP}$ is expressed as follows:

$$I_{K,ATP} = g_0 \left(\frac{[K^+]_o}{5.4} \right)^{0.24} f_M f_N f_T f_{ATP} (V - E_K), \quad (1)$$

where g_0 represents the maximum channel conductance (nS); $[K^+]_o$ is the extracellular concentration of K⁺ (mmol/L); factors f_M , f_N , f_T respectively denote the effects of intracellular Mg²⁺, Na⁺, and temperature. V and E_K represent the membrane potential and reverse potential of K⁺, respectively, (mV); and f_{ATP} is the fraction of opened channels. The model was further modified to incorporate species- and cell-type dependence and validated on available experimental data (see **Supplementary Figure 1**).

Modeling Effects of Exogenous H₂S on Ion Channels

In experiments, NaHS was used in most cases as H₂S donor rather than the direct administration of H₂S. Therefore, our simulations were based on experimental data of NaHS. Experimental data have shown that NaHS increased K-ATP, whereas it reduced the Ca-L channel current in rat cardiac cells. Therefore, the dose-dependent effect of NaHS on $I_{K,ATP}$ and I_{CaL} was modeled by the following:

$$I_{K,ATP}^{NaHS} = \left(1 + \frac{0.71}{1 + (K_{m,KATP}/NaHS)^{0.95}} \right) I_{K,ATP} \quad (2)$$

$$I_{CaL}^{NaHS} = \left(1 - \frac{0.7}{1 + (K_{m,CaL}/NaHS)^{0.77}} \right) I_{CaL} \quad (3)$$

These equations were fitted to experimental data (Sun et al., 2008; Zhong et al., 2010; Zhang et al., 2012), resulting in $K_{m,KATP}$ as 28.57 μmol/L and $K_{m,CaL}$ as 376.66 μmol/L. Fitting results and experimental data are available in **Supplementary Figure 2**.

Single-Cell Model

Healthy Rat Ventricular Myocyte Model

The above-described $I_{K,ATP}$ was incorporated into the Pandit et al. (2001) model [with corrected equations by Terkildsen et al. (2008)] for the AP of rat ventricular myocytes. $[ATP]_i$ and $[ADP]_i$ were set to 6,800 and 15 $\mu\text{mol/L}$ for healthy tissues (i.e., normoxic condition) based on measured nucleotide data as reported in a previous study (Weiss et al., 1992). APs were evoked in a same way as Pandit et al. (2001), that is, by a series of supra-threshold stimuli (S1; 1 Hz) with an amplitude of 0.6 nA and duration of 5 ms. Detailed methods on measuring APD, ERP, and excitability using the model are described in the **Supplementary Material**.

Ischemic Rat Ventricular Myocyte Model

For simulating the effect of ischemia on cellular APs, three major conditions were considered (i.e., hyperkalemia, anoxia, and acidosis), as considered in Shaw and Rudy's study (Shaw and Rudy, 1997). Simulations of the effect of 10-min ischemia on nucleotide concentrations, ion concentrations, and channel current conductance are detailed as follows:

Hyperkalemia

$$[K^+]_o = 8.0 \text{ mmol/L} \quad (4)$$

The elevated extracellular K^+ were based on rat experimental data as reported in Fiolet et al. (1984), Knopf et al. (1990) and Wilde et al. (1990).

Acidosis

$$g_{Na,acid} = 0.75 \cdot g_{Na} \quad (5)$$

$$g_{CaL,acid} = 0.75 \cdot g_{CaL} \quad (6)$$

Conductance reduction of these two channels was based on the observations in rat ventricular myocytes (Yatani and Goto, 1983; Yatani et al., 1984).

Anoxia

$$[ATP]_i = 4,600 \text{ } \mu\text{mol/L} \quad (7)$$

$$[ADP]_i = 99 \text{ } \mu\text{mol/L} \quad (8)$$

$$P_{CaL,ATP} = \frac{1}{1 + \left(\frac{K_m}{[ATP]_i}\right)^H} \quad (9)$$

Data of nucleotide levels in ischemia were obtained from Weiss et al. (1992). $P_{CaL,ATP}$ represents the influence of anoxia on the open fraction of Ca-L channel; and $K_m = 1,400 \text{ } \mu\text{mol/L}$ and $H = 2.6$. The effects of the above modifications on AP configurations were validated for epicardial and endocardial myocytes using available experimental data. Detailed validation results are presented later in this section.

In addition to the 10-min ischemia model, an earlier phase of ischemia was also considered for a transient stage in 2D simulation. The parameters for the ischemic condition during the transient stage are as follows:

$$[K^+]_o = 6.4 \text{ mmol/L} \quad (10)$$

$$g_{Na,acid} = 0.85 \cdot g_{Na} \quad (11)$$

$$g_{CaL,acid} = 0.85 \cdot g_{CaL} \quad (12)$$

$$[ATP]_i = 5500 \text{ } \mu\text{mol/L} \quad (13)$$

$$[ADP]_i = 64.6 \text{ } \mu\text{mol/L} \quad (14)$$

The relationship between $[ATP]_i$ and $[ADP]_i$ was calculated by fitting the calculation function proposed by Bao et al. (2013).

Validation of Single-Cell Model for Control and Ischemic Conditions

Validations of the developed single-cell model of the rat ventricular APs are shown in **Figure 6** for the control and ischemic conditions. The simulated ischemic condition as stated above based on the work of Shaw and Rudy (1997) abbreviated APs in both epicardial and endocardial myocytes; decreased their APA, maximum upstroke velocity (dV/dt_{max}), and CV (measured in 1D tissue strand model); but elevated the resting potential from -80 to around -71 mV. These simulated effects of ischemic condition matched well to experimental observations from rat and other species (Bélichard et al., 1991; De Diego et al., 2008), validating the developed rat ventricle cell models. Validation results are illustrated in **Figure 6**. All the data sources are available in **Supplementary Table 1**.

Transmural Ventricular Tissue Model

A multicellular tissue model for simulating the AP propagation was constructed using the well-established mono-domain equation (Clayton et al., 2011):

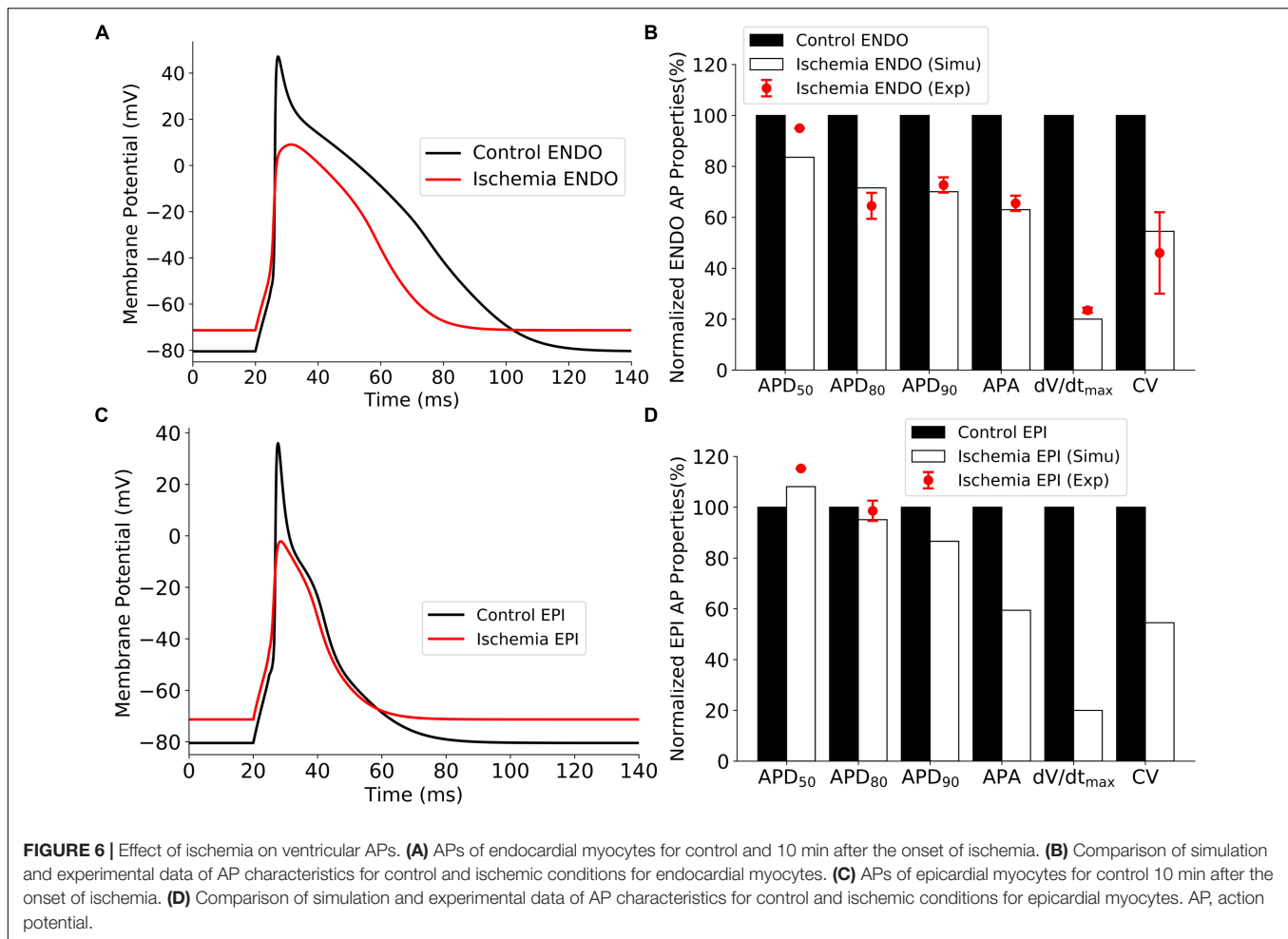
$$\frac{\partial V_m}{\partial t} = \nabla \cdot (\mathbf{D} \nabla V_m) - \frac{I_{ion}}{C_m} \quad (15)$$

where \mathbf{D} is the diffusion coefficient matrix describing the intercellular electrical coupling via gap junctions. When considering the 1D tissue strand, Eq. 15 can be further organized as follows:

$$\frac{\partial V_m}{\partial t} = D \left(\frac{\partial^2 V_m}{\partial x^2} \right) - \frac{I_{ion}}{C_m} \quad (16)$$

where D is a scalar value that is set to $1.8 \times 10^{-2} \text{ mm}^2/\text{ms}$ in the 1D tissue model, giving a transmural CV of 19.84 cm/s, within the measured range of 14.6 to 102 cm/s in rat ventricular tissues (Sedmera et al., 2016). As the ventricular wall in rat heart is rather thin, a length of 3 mm of transmural 1D strand was constructed with 2 mm designated as endocardial and 1 mm epicardial tissues, which was inconsistent with our previous study (Zhang et al., 2009). The spatial resolution dx was set to 0.1 mm, close to the length of single ventricular myocyte (80–150 μm); thus, the constructed strand contained 20 nodes for endocardial and 10 nodes for epicardial tissues.

The 2D transmural tissue model was constructed by expanding the 1D strand in the y direction, thus forming a



$3 \times 10 \text{ mm}^2$ tissue sheet. The spatial resolution in the y direction dy is the same as dx . Anisotropic cell-to-cell electrical coupling CV was assumed in this study. Specifically, the fiber orientation was set to vertical, and the diffusion coefficients were set to $1.8 \times 10^{-2} \text{ mm}^2/\text{ms}$ in the fiber orientation and $7.2 \times 10^{-2} \text{ mm}^2/\text{ms}$, which were perpendicular to the fiber orientation [i.e., coefficient ratio $D_{\perp}:D_{\parallel} = 1:4$ according to Benson et al. (2008)]. The above settings gave a transmural CV of 19.84 cm/s and a longitudinal CV of 41.97 cm/s, approximately in a ratio of 1:2 in healthy tissues. In the ischemic condition, the coefficient was decreased by 20% to mimic the reduced intercellular coupling.

Measurement of Vulnerability to Unidirectional Conduction Block – Temporal Vulnerability

Temporal vulnerability to reentrant arrhythmia was quantitatively measured as the width of VW in 1D tissue model. Standard S1–S2 protocol (Zhang et al., 2009) was used. Specifically, supra-threshold stimuli (S1) were applied to the 0.3-mm segment at the endocardial end for five times at 1 Hz. Then a premature stimulus S2 was applied to a 0.6-mm segment with a time delay Δt after S1. At a certain period that just

after the refractory tail of S1 induced AP wavefront, S2 could produce a solitary wave that propagated in the anterograde but not retrograde direction, or vice versa. This was due to the different refractory durations between two directions. If S2 was applied too early, propagation failed in both directions and unidirectional conduction block could not be formed. On the other hand, if it was applied too late, bidirectional conduction could occur. The time period during which a S2 stimulus evoked unidirectional conduction block is referred to as VW.

Vulnerable window at each point in the 1D strand (except the 0.3-mm segments at the two ends of strand owing to the 0.6-mm stimulating length) was measured. In our simulation, the S1–S2 protocol was iteratively performed for every point until VWs across all strand were determined. The S1 stimuli were always applied to the first 0.3-mm endocardial segment in every measurement. As for the premature stimulus S2, the stimulating length was 0.6 mm, but its location was not fixed because every point on the strand had its own VW distribution that is to be determined in the simulation. For any given point, noted x , S2 was given to the segment from $(x-0.3) \text{ mm}$ to $(x+0.3) \text{ mm}$ after the S1 stimulus was applied. The interval between S2 and the last S1 (termed S1–S2 interval) was also not fixed, and different S1–S2 intervals would produce bidirectional conduction block

(S2 too early), bidirectional conduction block (S2 too late), or unidirectional conduction block (S2 in VW). The time duration that S2 produced unidirectional conduction block was recorded as the width of VW for the point x .

Measurement of Critical Size of Tissue to Support Reentry – Spatial Vulnerability

Using a similar S1–S2 protocol in 2D tissues may initiate the reentrant excitation wave. S1 stimuli were applied to the first 0.3 mm of cells in endocardial side (left side) for five times at 1 Hz. Then the premature stimulus S2 was applied during the VW to a local vertical area at the bottom of the tissues, with fixed width of 0.6 mm and variable length (or height) from 3.0 to 8.0 mm. The center of stimulated area was 1.3 mm away from the endocardial side (left side) and was consistent in all cases (i.e., control, NaHS, ischemia, and ischemia + NaHS) to avoid location-dependent variation.

During VW, excitation wave evoked by S2 stimulus could be unidirectional conduction, which evolves into spiral wave. However, the spiral wave could sustain only when a sufficient length of S2 was given, as the spiral wave required space to survive. Or if the length of S2 was too small, the tip of the spiral wave would hit the bottom boundary of the tissues and would self-terminate. Therefore, a certain length (termed *critical length*) could represent the spatial vulnerability of tissues to reentry.

In 2D simulations, an earlier phase of ischemia was also considered, with mild hyperkalemia from 5.4 to 6.4 mmol/L, 15% decrease of calcium and sodium channel conductance, and a reduction of intracellular ATP from 6,800 to 5,500 $\mu\text{mol/L}$. Equations in this condition are listed in *Ischemic Rat Ventricular Myocyte Model*, that is, Eqs 10–14.

REFERENCES

- Abramochkin, D. V., Moiseenko, L. S., and Kuzmin, V. S. (2009). The effect of hydrogen sulfide on electrical activity of rat atrial myocardium. *Bull. Exp. Biol. Med.* 147, 683–686. doi: 10.1007/s10517-009-0607-y
- Bao, L., Taskin, E., Foster, M., Ray, B., Rosario, R., Ananthkrishnan, R., et al. (2013). Alterations in ventricular KATP channel properties during aging. *Aging Cell* 12, 167–176. doi: 10.1111/acel.12033
- Bates, M. N., Garrett, N., and Shoemack, P. (2002). Investigation of health effects of hydrogen sulfide from a geothermal source. *Arch. Environ. Health* 57, 405–411. doi: 10.1080/00039890209601428
- Bélichard, P., Pruneau, D., Rouet, R., and Salzmann, J. L. (1991). Electrophysiological responses of hypertrophied rat myocardium to combined hypoxia, hyperkalemia, and acidosis. *J. Cardiovasc. Pharmacol.* 17, S141–S145.
- Benson, A. P., Aslanidi, O. V., Zhang, H., and Holden, A. V. (2008). The canine virtual ventricular wall: a platform for dissecting pharmacological effects on propagation and arrhythmogenesis. *Prog. Biophys. Mol. Biol.* 96, 187–208. doi: 10.1016/j.pbiomolbio.2007.08.002
- Bernus, O., Zemlin, C. W., Zaritsky, R. M., Mironov, S. F., and Pertsov, A. M. (2005). Alternating conduction in the ischaemic border zone as precursor of reentrant arrhythmias: a simulation study. *Europace* 7, S93–S104.
- Bian, J.-S., Yong, Q. C., Pan, T.-T., Feng, Z.-N., Ali, M. Y., Zhou, S., et al. (2006). Role of hydrogen sulfide in the cardioprotection caused by ischemic preconditioning in the rat heart and cardiac myocytes. *J. Pharmacol. Exp. Ther.* 316, 670–678. doi: 10.1124/jpet.105.092023
- Chan, C.-S., Lin, Y.-K., Kao, Y.-H., Chen, Y.-C., Chen, S.-A., and Chen, Y.-J. (2018). Hydrogen sulphide increases pulmonary veins and atrial arrhythmogenesis

DATA AVAILABILITY STATEMENT

All datasets generated for this study are included in the article/**Supplementary Material**.

AUTHOR CONTRIBUTIONS

HZ and ZW conceptualized the idea of the manuscript. HZ provided the basic mythological structure. SGZ, SZZ, and XF developed the relevant codes in the single-cell model. SGZ, XF, and WW developed the relevant codes in 1D and 2D tissue models. HZ, SZZ, ZL, and DJ analyzed the simulation results, including the validation of cell model output and the spiral wave results. SGZ drafted the original manuscript. SGZ, HZ, and ZW wrote the manuscript.

FUNDING

This work was supported by the China Scholarship Council (CSC) and by grants from EPSRC (United Kingdom) (EP/J00958X/1 and EP/I029826/1), MC-IRSES CORDIS3D (317766), and NSFC (61179009).

SUPPLEMENTARY MATERIAL

The Supplementary Material for this article can be found online at: <https://www.frontiersin.org/articles/10.3389/fphys.2019.01482/full#supplementary-material>

- with activation of protein kinase C. *J. Cell Mol. Med.* 22, 3503–3513. doi: 10.1111/jcmm.13627
- Clayton, R. H., Bernus, O., Cherry, E. M., Dierckx, H., Fenton, F. H., Mirabella, L., et al. (2011). Models of cardiac tissue electrophysiology: progress, challenges and open questions. *Prog. Biophys. Mol. Biol.* 104, 22–48. doi: 10.1016/j.pbiomolbio.2010.05.008
- Comtois, P., Kneller, J., and Nattel, S. (2005). Of circles and spirals: bridging the gap between the leading circle and spiral wave concepts of cardiac reentry. *Europace* 7, S10–S20.
- De Diego, C., Pai, R. K., Chen, F., Xie, L.-H., De Leeuw, J., Weiss, J. N., et al. (2008). Electrophysiological consequences of acute regional ischemia/reperfusion in neonatal rat ventricular myocyte monolayers. *Circulation* 118, 2330–2337. doi: 10.1161/CIRCULATIONAHA.108.789149
- Ferrero, J. M., Sáiz, J., and Thakor, N. V. (1996). Simulation of action potentials from metabolically impaired cardiac myocytes: role of ATP-sensitive K^+ current. *Circ. Res.* 79, 208–221. doi: 10.1161/01.res.79.2.208
- Finnbjornsdottir, R. G., Carlsen, H. K., Thorsteinsson, T., Oudin, A., Lund, S. H., Gislason, T., et al. (2016). Association between daily hydrogen sulfide exposure and incidence of emergency hospital visits: a population-based study. *PLoS One* 11:e0154946. doi: 10.1371/journal.pone.0154946
- Finnbjornsdottir, R. G., Oudin, A., Elvarsson, B. T., Gislason, T., and Rafnsson, V. (2015). Hydrogen sulfide and traffic-related air pollutants in association with increased mortality: a case-crossover study in Reykjavik, Iceland. *BMJ Open* 5:e007272. doi: 10.1136/bmjopen-2014-007272
- Fiolet, J. W. T., Baartscheer, A., Schumacher, C. A., Coronel, R., and Ter Welle, H. F. (1984). The change of the free energy of ATP hydrolysis during global ischemia and anoxia in the rat heart: Its possible role in the regulation of

- transsarcolemmal sodium and potassium gradients. *J. Mol. Cell. Cardiol.* 16, 1023–1036. doi: 10.1016/s0022-2828(84)80015-2
- Fiordelisi, A., Piscitelli, P., Trimarco, B., Coscioni, E., Iaccarino, G., and Sorriento, D. (2017). The mechanisms of air pollution and particulate matter in cardiovascular diseases. *Heart Fail. Rev.* 22, 337–347. doi: 10.1007/s10741-017-9606-7
- Furukawa, T., Kimura, S., Furukawa, N., Bassett, A. L., and Myerburg, R. J. (1991). Role of cardiac ATP-regulated potassium channels in differential responses of endocardial and epicardial cells to ischemia. *Circ. Res.* 68, 1693–1702. doi: 10.1161/01.res.68.6.1693
- Gattoni, S., Røe, Å.T., Frisk, M., Louch, W. E., Niederer, S. A., and Smith, N. P. (2016). The calcium–frequency response in the rat ventricular myocyte: an experimental and modelling study. *J. Physiol.* 594, 4193–4224. doi: 10.1113/JP272011
- Godleski, J. J., Verrier, R. L., Koutrakis, P., Catalano, P., Coull, B., Reinisch, U., et al. (2000). Mechanisms of morbidity and mortality from exposure to ambient air particles. *Res. Rep. Health Eff. Inst.* 91, 5–88.
- Johansen, D., Ytrehus, K., and Baxter, G. F. (2006). Exogenous hydrogen sulfide (H₂S) protects against regional myocardial ischemia–reperfusion injury. *Basic Res. Cardiol.* 101, 53–60. doi: 10.1007/s00395-005-0569-9
- Knopf, H., Theising, R., Moon, C. H., and Hirche, H. J. (1990). Continuous determination of extracellular space and changes of K⁺, Na⁺, Ca²⁺, and H⁺ during global ischaemia in isolated rat hearts. *J. Mol. Cell. Cardiol.* 22, 1259–1272. doi: 10.1016/0022-2828(90)90062-7
- Link, M. S., and Dockery, D. W. (2010). Air pollution and the triggering of cardiac arrhythmias. *Curr. Opin. Cardiol.* 25, 16–22. doi: 10.1097/HCO.0b013e32833358cd
- Martinelli, N., Olivieri, O., and Girelli, D. (2013). Air particulate matter and cardiovascular disease: a narrative review. *Eur. J. Intern. Med.* 24, 295–302. doi: 10.1016/j.ejim.2013.04.001
- Mills, N. L., Donaldson, K., Hadoke, P. W., Boon, N. A., MacNee, W., Cassee, F. R., et al. (2009). Adverse cardiovascular effects of air pollution. *Nat. Clin. Pract. Cardiovasc. Med.* 6, 36–44. doi: 10.1038/ncpcardio1399
- Pandit, S. V., Clark, R. B., Giles, W. R., and Demir, S. S. (2001). A mathematical model of action potential heterogeneity in adult rat left ventricular myocytes. *Biophys. J.* 81, 3029–3051. doi: 10.1016/s0006-3495(01)75943-7
- Picard, S., Rouet, R., Ducouret, P., Puddu, P. E., Flais, F., Criniti, A., et al. (1999). KATP channels and 'border zone' arrhythmias: role of the repolarization dispersion between normal and ischaemic ventricular regions. *Br. J. Pharmacol.* 127, 1687–1695. doi: 10.1038/sj.bjp.0702704
- Qi, X. Y., Shi, W. B., Wang, H. H., Zhang, Z. X., and Xu, Y. Q. (2000). A study on the electrophysiological heterogeneity of rabbit ventricular myocytes the effect of ischemia on action potentials and potassium currents. *Sheng Li Xue Bao* 52, 360–364.
- Rensma, P. L., Alessie, M. A., Lammers, W. J., Bonke, F. I., and Schalij, M. J. (1988). Length of excitation wave and susceptibility to reentrant atrial arrhythmias in normal conscious dogs. *Circ. Res.* 62, 395–410. doi: 10.1161/01.res.62.2.395
- Schlesinger, R. B. (2007). The health impact of common inorganic components of fine particulate matter (PM_{2.5}) in ambient air: a critical review. *Inhal. Toxicol.* 19, 811–832. doi: 10.1080/08958370701402382
- Sedmera, D., Neckar, J., Benes, J. Jr., Pospisilova, J., Petrak, J., Sedlacek, K., et al. (2016). Changes in myocardial composition and conduction properties in rat heart failure model induced by chronic volume overload. *Front. Physiol.* 7:367. doi: 10.3389/fphys.2016.00367
- Shaw, R. M., and Rudy, Y. (1997). Electrophysiologic effects of acute myocardial ischemia: a theoretical study of altered cell excitability and action potential duration. *Cardiovasc. Res.* 35, 256–272. doi: 10.1016/s0008-6363(97)00093-x
- Shimokawa, J., Yokoshiki, H., and Tsutsui, H. (2007). Impaired activation of ATP-sensitive K⁺ channels in endocardial myocytes from left ventricular hypertrophy. *Am. J. Physiol. Circ. Physiol.* 293, H3643–H3649.
- Sun, Y.-G., Cao, Y.-X., Wang, W.-W., Ma, S.-F., Yao, T., and Zhu, Y.-C. (2008). Hydrogen sulphide is an inhibitor of L-type calcium channels and mechanical contraction in rat cardiomyocytes. *Cardiovasc. Res.* 79, 632–641. doi: 10.1093/cvr/cvn140
- Terkildsen, J. R., Niederer, S., Crampin, E. J., Hunter, P., and Smith, N. P. (2008). Using Physiome standards to couple cellular functions for rat cardiac excitation–contraction. *Exp. Physiol.* 93, 919–929. doi: 10.1113/expphysiol.2007.041871
- Trénor, B., Romero, L., Ferrero, J. M., Sáiz, J., Moltó, G., and Alonso, J. M. (2007). Vulnerability to reentry in a regionally ischemic tissue: a simulation study. *Ann. Biomed. Eng.* 35, 1756–1770. doi: 10.1007/s10439-007-9353-3
- Weiss, J. N., Venkatesh, N., and Lamp, S. T. (1992). ATP-sensitive K⁺ channels and cellular K⁺ loss in hypoxic and ischaemic mammalian ventricle. *J. Physiol.* 447, 649–673. doi: 10.1113/jphysiol.1992.sp019022
- Wilde, A. A. M., Escande, D., Schumacher, C. A., Thuringer, D., Mestre, M., Fiolet, J. W. T., et al. (1990). Potassium accumulation in the globally ischemic mammalian heart. A role for the ATP-sensitive potassium channel. *Circ. Res.* 67, 835–843. doi: 10.1161/01.res.67.4.835
- Yatani, A., Brown, A. M., and Akaike, N. (1984). Effect of extracellular pH on sodium current in isolated, single rat ventricular cells. *J. Membr. Biol.* 78, 163–168. doi: 10.1007/bf01869203
- Yatani, A., and Goto, M. (1983). The effect of extracellular low pH on the plateau current in isolated, single rat ventricular cells—A voltage clamp study. *Jpn. J. Physiol.* 33, 403–415. doi: 10.2170/jjphysiol.33.403
- Zhang, H., Kharche, S., Holden, A. V., and Hancox, J. C. (2008). Repolarisation and vulnerability to re-entry in the human heart with short QT syndrome arising from KCNQ1 mutation—A simulation study. *Prog. Biophys. Mol. Biol.* 96, 112–131. doi: 10.1016/j.pbiomolbio.2007.07.020
- Zhang, H., Tao, T., Kharche, S., and Harrison, S. M. (2009). Modelling changes in transmural propagation and susceptibility to arrhythmia induced by volatile anaesthetics in ventricular tissue. *J. Theor. Biol.* 257, 279–291. doi: 10.1016/j.jtbi.2008.12.004
- Zhang, R., Sun, Y., Tsai, H., Tang, C., Jin, H., and Du, J. (2012). Hydrogen sulfide inhibits L-type calcium currents depending upon the protein sulfhydryl state in rat cardiomyocytes. *PLoS One* 7:e37073. doi: 10.1371/journal.pone.0037073
- Zhang, Z., Huang, H., Liu, P., Tang, C., and Wang, J. (2007). Hydrogen sulfide contributes to cardioprotection during ischemia–reperfusion injury by opening KATP channels. *Can. J. Physiol. Pharmacol.* 85, 1248–1253. doi: 10.1139/y07-120
- Zhong, G., Chen, F., Cheng, Y., Tang, C., and Du, J. (2003). The role of hydrogen sulfide generation in the pathogenesis of hypertension in rats induced by inhibition of nitric oxide synthase. *J. Hypertens* 21, 1879–1885. doi: 10.1097/00004872-200310000-00015
- Zhong, G.-Z., Li, Y.-B., Liu, X.-L., Guo, L.-S., Chen, M., and Yang, X.-C. (2010). Hydrogen sulfide opens the KATP channel on rat atrial and ventricular myocytes. *Cardiology* 115, 120–126. doi: 10.1159/000260073

Conflict of Interest: The authors declare that the research was conducted in the absence of any commercial or financial relationships that could be construed as a potential conflict of interest.

Copyright © 2019 Zhang, Zhang, Fan, Wang, Li, Jia, Wei and Zhang. This is an open-access article distributed under the terms of the Creative Commons Attribution License (CC BY). The use, distribution or reproduction in other forums is permitted, provided the original author(s) and the copyright owner(s) are credited and that the original publication in this journal is cited, in accordance with accepted academic practice. No use, distribution or reproduction is permitted which does not comply with these terms.